Colloids and Surfaces A: Physicochemical and Engineering Aspects 626 (2021) 127009

Contents lists available at ScienceDirect

Colloids and Surfaces A: Physicochemical and Engineering Aspects

journal homepage: www.elsevier.com/locate/colsurfa

Foamability of surfactant solutions: Interplay between adsorption and hydrodynamic conditions

B. Petkova, S. Tcholakova *, N. Denkov

Department of Chemical and Pharmaceutical Engineering, Faculty of Chemistry and Pharmacy, Sofia University, 1 J. Bourchier Ave., 1164 Sofia, Bulgaria

GRAPHICAL ABSTRACT

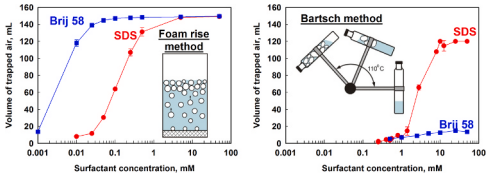

ARTICLE INFO

Keywords:
Foaming
Foam test
Bartsch test
Bubbling test
Dynamic adsorption layer

ABSTRACT

The foamability of surfactant solutions depends strongly on the adsorption properties of the surfactants, their concentrations, and the foaming test used for foam generation. The aim of the current study is to analyse the subtle interplay between the hydrodynamic conditions and the surfactant adsorption layers formed during foaming. We compare the results from three foam tests, characterized with very different hydrodynamic conditions. The Bartsch test (fast-foaming method) is characterized by a very short time, of the order of milliseconds, allowed for surfactant adsorption before the newly generated bubbles collide with each other. The other two "slow-foaming" tests, the planetary mixer and the foam rise method, are very different from this viewpoint – the characteristic time for surfactant adsorption before the bubble collisions is much longer, of the order of seconds. Surfactants of two different types, nonionic and anionic, with different chain-lengths are compared. The obtained results reveal that the long-chain nonionic surfactants with 16 carbon atoms are unable to stabilize the foams in the fast-foaming test, even at very high surfactant concentrations (50 mM), due to their relatively slow adsorption. Interestingly, the same surfactants are excellent foam stabilizers in the slow-foaming tests. On the other hand, the medium-chain anionic surfactants with 12 carbon atoms are very suitable for stabilization of the gas bubbles in the fast-foaming test, even at relatively low concentrations, due to their rapid adsorption and inherent electrostatic repulsion. In slow-foaming tests, however, the anionic surfactants show lower foamability to the nonionic ones. All results from the foam tests are explained in a unified approach which accounts explicitly for the rate of surfactant adsorption and for the characteristic time-scales of the various foaming tests.

1. Introduction

The foamability of surfactant solutions is widely studied in the literature due to its importance in froth flotation [1–6], food industry [7–11], cleaning applications and personal care [12–14], bioreactors [15–17], etc. The conditions for foam generation differ significantly, depending on the practical demand and, therefore, various foaming tests have been developed and used to mimic the conditions in the real

* Corresponding author.
E-mail address: SC@LCPE.UNI-SOFIA.BG (S. Tcholakova).

https://doi.org/10.1016/j.colsurfa.2021.127009
Received 11 April 2021; Received in revised form 3 June 2021; Accepted 8 June 2021
Available online 10 June 2021

applications [18–21]. The foaming tests can be divided into two large groups, depending on the mode of gas supply: (1) Methods in which the gas is introduced under pressure and the rate of gas supply can be controlled by the operator, and (2) Methods with mechanical stirring of the solution where the air is entrapped into the foam from the atmosphere. The first group of methods includes the various sparging tests, in which the gas is blown through a porous disc, set of capillaries, or set of needles [18, 22–26], and the steam ejection devices [27–29]. The second group includes tests in which the gas is entrapped via the formation of hydrodynamic waves of large amplitude on the solution surface – these include the planetary mixers [30–32], rotor-stator mixers [33,34], Bartsch test [35–38], Ross-Miles test [39–41], continuous plunging jet method [42] and shake machines [24,43].

In our previous study we showed that the foamability in a Kenwood mixer at high surfactant concentration strongly depends on the viscosity of the foamed solution and on the surface properties of the surfactant [32]. A subtle interplay between the amount of entrapped air and the rheological properties of the generated foam has been established [32]. These results were explained with reaching a critical value of the shear stress of the generated foam, above which the formation of surface waves and the related air entrapment are blocked [32].

In a separate study [38] we showed that the foamability of various surfactant solutions in the Bartsch test is controlled by the coverage of the bubble surfaces by surfactant and by the surfactant charges which induce electrostatic repulsion between the entrapped bubbles for the ionic surfactants. The surface coverage on its turn depends on the rate of surfactant adsorption and can be determined from the measured dynamic surface tension of the foamed solutions. Two master curves were found to describe the experimental data for the ionic and nonionic surfactants, respectively, in these experiments [38].

Comparing the results from different foam tests, non-trivial differences are observed for the foamability of the same surfactant solutions. For example, the foamability of the long-chain nonionic surfactant Tween 60 was observed to be very low in the Bartsch test [38], whereas the same surfactant gave excellent foam in a sparging test [40]. Other studies also showed that the hydrodynamic conditions during foaming could affect strongly the final foam volume and the bubble size for a given surfactant solution [22].

The major aim of the current study is to develop a general approach for comparing the foaming results obtained in different foam tests with different surfactant solutions. To achieve this aim, we performed systematic series of experiments with three surfactants, applied in wide range of concentrations, in three foaming tests, characterized with very different dynamics of bubble generation: foam rise method (FRM), planetary mixer and Bartsch test, Fig. 1. The surface properties of the studied surfactant solutions have been previously characterized [38] by the maximum bubble pressure method and the equilibrium surface tension isotherm, and are used here to interpret quantitatively the obtained results from the various foam tests, adapting the theoretical approach developed and applied for the Bartsch test only in Ref. [38]. Non-trivial results and conclusions are formulated, which reveal the important role of the specific foam test and of the hydrodynamic conditions during foaming on the selection of the appropriate surfactant (ionic or nonionic, medium-chain or long-chain) for ensuring voluminous and stable foam.

2. Materials and methods

2.1. Materials

Three surfactants were systematically studied and compared: the anionic sodium dodecyl sulfate (SDS with C_{12} tail, product of Acros) and two nonionic (Sigma) – polyoxyethylenesorbitan monolaurate (Tween 20, also with C_{12}) and polyoxyethylene-20 cetyl ether (Brij 58 with C_{16} tail). For comparison, in several series of experiments we studied also the non-ionic surfactant polyoxyethylenesorbitan monopalmitate (Tween 40 with C_{16} tail). All surfactants were of purity > 98% and were used as received. All solutions were prepared with deionized water produced from Millipore Elix system.

2.2. Foamability of the solutions studied

2.2.1. Automated Bartsch test

We used an automated Bartsch test (shaken cylinder), described in detail in Ref. [38]. In our experiments, the shaking period was 1.23 s (frequency = 0.813 s^{-1}) and the volume of the surfactant solution was 10 mL, contained in a glass cylinder of 120 mL. The foamability of the studied systems was characterized by the volume of trapped air, V_A,

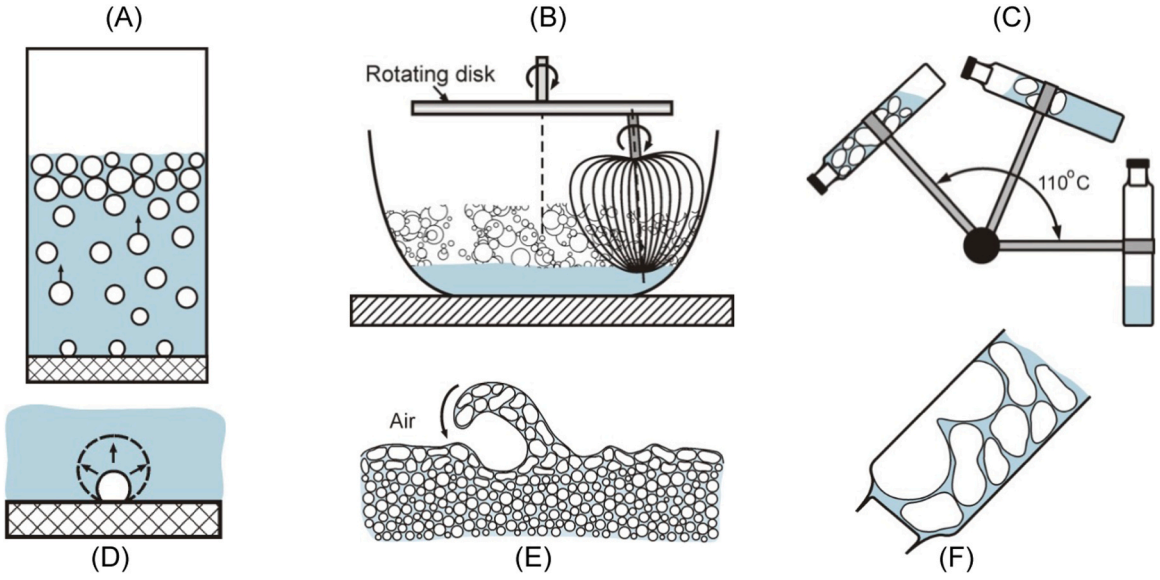

Fig. 1. Schematic presentation of (A) Foam rise method (FRM), called also "bubbling test"; (B) Planetary mixer, and (C) Automated Bartsch test, used in the current study. (D)-(F) Main process of bubble formation in the respective test. Note that the bubble surface remains almost fixed after the bubbles are released from the bottom of the surfactant solution in the FRM, whereas the bubble surface area can vary significantly during foaming in the planetary mixer and in the Bartsch test, due to the strong shear and inertial forces in these two tests.

calculated by subtracting the solution volume (10 mL) from the total volume (solution + foam) measured during the test. We measured V_A in the foam, generated after 3, 5, 10, 20, 30, 50 and 100 consecutive shake cycles, thus characterizing the initial rate of foam formation and the foam accumulation with the foaming time. The experiments were performed at $T = 20 \pm 1$ °C.

2.2.2. Planetary mixer

We used planetary mixer Kenwood Chef Premier KMC 560 (1000 W). The geometrical parameters of this mixer are described in detail in Ref. [32]. The surfactant solution with volume, V_0, was placed in a transparent vessel with total volume of 3250 mL. The mixing tool was rotated with a speed of 2 rotations per second (rps). This rotation speed creates a maximum shear rate in the vessel of 62 s^{-1}, as explained in Ref. [32]. The volume of the generated foam was monitored as a function of the shearing time. After a certain period of shearing, the foam volume stopped increasing. To be sure that the maximum foam volume was reached, we continued the foam shearing for 5 additional minutes. The foams obtained at the end of the shearing period were characterized in terms of their volume, average bubble size, and air volume fraction.

2.2.3. Foam rise method

We used Dynamic Foam Analyzer DFA100 (Krüss GmbH, Germany). In this instrument, the foam is formed by bubbling of gas through a glass porous frit into the foaming solution. The frit is mounted at the base of a glass cylinder of 40 mm inner diameter and 250 mm height. The height of the foam and of the liquid layer (below the foam) was detected and recorded automatically by computer-controlled linear LED panel and a line sensor mounted along the column height. The volume of the trapped air was calculated as a difference between the upper foam level and the initial solution volume. We used CY4572 prism column that enabled us to measure the bubble size distribution in the foam formed. This instrument gives information about the foam height, the liquid content in the foam and the bubble size. The foaming procedure was as follows: 50 mL of the surfactant solution was poured into the cylinder and the gas was supplied under pressure for 10 s, with a flow rate varied in the separate experiments (0.27 denoted for brevity as 0.3 L/min in the text and figures; 0.57 denoted as 0.6 L/min in the text and figures or 0.88 L/min denoted as 0.9 L/min in the text and figures) through a frit of porosity G2 (40–100 μm pore size). The foam decay was recorded for 200 s after stopping the gas supply.

The initial jump in the foamability from 0 to 5–6 mL in the first hundreds of ms is related to the very rapid mixing upon starting the gas supply and the inability of the used equipment to detect the exact position of the upper interface. Therefore, the first point in the graph is the foam volume measured after 1 s of foam generation where the upper level is well defined.

2.3. Determination of bubble size in the foams generated in the Kenwood mixer

Bubble size distribution in the final foams, generated in the Kenwood mixer, was determined by the method of Garrett et al. [32,44]. The foam was spread in a small petri dish and an optical triangular prism was placed on top, in direct contact with the foam. The foam was illuminated by diffuse white light through one of the prism side-walls, whereas the observation was made by video camera, through the other side-wall of the prism. In the recorded images one sees the wetting films, formed between the bubbles and the prism wall, as bright polygonal spots, whereas the Plateau borders around the films are seen as dark interconnected areas. The foam images were processed via an open software package ImageJ, released by the National Institute of Health (NIH) [45]. For scaling the rheological data, the mean surface-volume radius, R_{32}, called also Sauter mean radius, was used:

$$R_{32} = \sum_i R_i^3 / \sum_i R_i^2 \quad (1)$$

where the sum is taken over all measured bubbles in a given sample.

2.4. Thin film behavior

We used the capillary cell of Scheludko-Exerowa to observe the behavior of foam films, formed from a biconcave drop the surfactant solution, placed in a short capillary, by sucking out this solution through a side orifice [46]. The observations were performed in reflected light by using optical microscope Axioplan (Zeiss, Germany), equipped with a long-distance objective Zeiss Epiplan 20 × /0.40, CCD camera (Sony) and digital video recorder. The foam films were observed for 15 min in a closed to the atmosphere cell to prevent the water evaporation from the foam film surfaces.

2.5. Measuring surface tension by Wilhelmy plate method

To determine the surface coverage on the bubble surfaces in the various foam tests we used the theoretical approach described in Ref. [38]. This approach requires knowing the equilibrium surface tension isotherms, $\sigma(C_S)$, of the surfactants studied (already presented in Ref. [38]) and the dynamic surface tensions of the foamed surfactant solutions, $\sigma_d(C_S,t)$. As explained in Section 3.4 below, the various foaming tests compared in the current study require different procedures for measuring the dynamic surface tension. The foaming in the Bartsch test and Kenwood mixer is adequately described by the dynamic surface tensions measured by the maximum bubble pressure method (MBPM); the respective results are also presented in Ref. [38] for all surfactants studied here. On the other hand, the dynamic surface tension of the same solutions should be measured by a method ensuring static (not expanding) solution surface for analysing the foaming data from the FRM. Therefore, in the current study we measured the dynamic surface tensions of the same surfactant solutions using the Wilhelmy plate method on K100 apparatus (Kruess, Germany) with the following procedure: (1) The solution was placed in glass vessel, thus creating a fresh solution surface; (2) After 30 s the platinum plate was placed in contact with the solution surface; (3) The surface tension was recorded for 300 additional seconds.

3. Experimental results and discussion

In the current section we describe the experimental results obtained in the three foam tests, Sections 3.1–3.3, and compare these results in Section 3.4.

3.1. Foamability in the Bartsch test

In our previous study [38] we showed that the ionic surfactants with 12 and 16 carbon atoms in their tails are able to form voluminous foam in the fast-foaming Bartsch test, whereas the long-chain nonionic surfactants (Tween 40 and Brij 58 with 16 carbon atoms) are unable to generate voluminous foam in this test. Illustrative results for the rate of foam generation at surfactant concentrations of 0.5, 5 and 50 mM are shown in Fig. 2. The experimental data are described well by the empirical equation proposed in Ref. [38]:

$$V_A(n) = V_{A\infty}[1 - \exp(-n/n_A)] \quad (2)$$

where $V_{A\infty}$ is the maximum volume of the air which would be entrapped after a very large number of cycles, n is the number of the respective cycle at which V_A is measured, and n_A is the characteristic number of cycles at which V_A reaches ≈ 63% of $V_{A\infty}$. Illustrative examples of the description of our experimental data by Eq. (2) are shown in Fig. 2A. As seen from this graph, the long-chain nonionic surfactant Brij 58 cannot

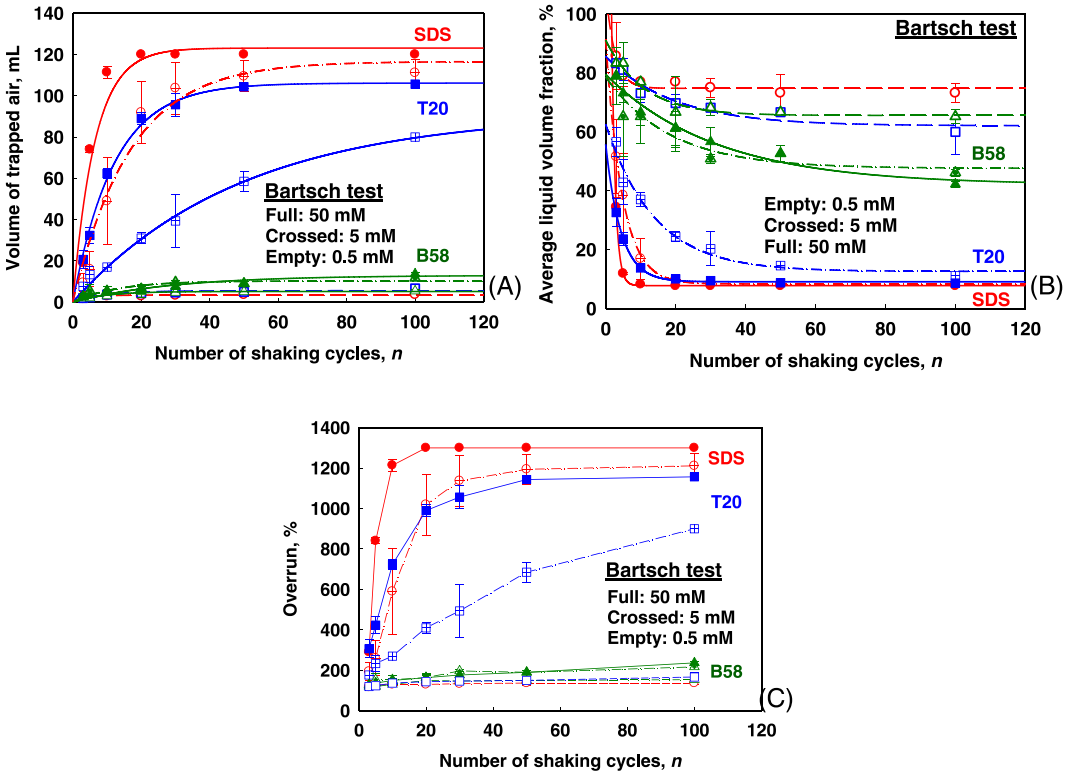

Fig. 2. Foaming in the Bartsch test: (A) Volume of the trapped air; (B) Mean average liquid fraction and (C) Overrun, as functions of the number of shake cycles, for solutions of the anionic surfactant SDS (red circles) and the nonionic Tween 20 (blue squares) and Brij 58 (green triangles), all surfactants studied at 0.5 mM (empty), 5 mM (crossed) and 50 mM (full symbols). The symbols show the experimental data, whereas the curves are fits by Eq. (2) in (A) and by Eq. (4) in (B). (For interpretation of the references to color in this figure legend, the reader is referred to the web version of this article.)

stabilize voluminous foam even at very high surfactant concentration of 50 mM, whereas the medium-chain nonionic Tween 20 and the anionic SDS are able to boost the foam volume at concentration of ≈ 5 mM. Note that the kinetics of air entrapment depends strongly on the type of surfactant used and its concentration – the initial rate of foaming is much higher with SDS when compared to Tween 20 (both with 12 carbon atoms in their chains).

Other two characteristics used in the literature to characterize the foamability of surfactant solutions are the average liquid volume fraction, Φ_L, and the overrun, Ω, defined as [47,48]:

$$\Phi_L = V_L/(V_L + V_A) \tag{3}$$

$$\Omega = V_A/V_L \tag{4}$$

Here V_L is the volume of the aqueous solution which is 10 mL in this test and V_A is the volume of trapped air. The average liquid volume fraction is shown in Fig. 2B as a function of the number of shaking cycles. One sees that the average liquid volume fraction $\Phi_L > 50\%$ for Brij 58 (16 carbon atoms) at all concentrations, whereas this is true for SDS and Tween 20 at low concentrations only. The decrease of Φ_L with the number of shaking cycles can be described by the following equation:

$$\Phi_L = \Phi_{L\infty} + \Phi_{L1}\exp(-n/n_L) \tag{5}$$

where $\Phi_{L\infty}$ is the final average liquid volume fraction, reached after very large number of shaking cycles and related to $V_{A\infty}$ by Eq. (3). The parameter n_L characterizes the rate of decrease of the average liquid volume fraction with the number of shaking cycles. Eq. (5) defines Φ_{L1} as a parameter for which $(\Phi_{L\infty} + \Phi_{L1}) = \Phi_L(n = 0) \approx 100\%$. For most of the studied systems this relation was satisfied very well with the values of $\Phi_{L\infty}$ and Φ_{L1}, determined from the best fits to the experimental data. However, for several most rapidly foaming solutions we found $(\Phi_{L\infty} + \Phi_{L1}) < 100\%$ which was an indication that very voluminous foam was formed even after the first shake cycle.

Note that the final average volume fraction $\Phi_{L\infty} < 10\%$ at high concentrations of the rapidly foaming solutions of SDS and Tween 20. This value means that the bubbles were strongly compressed in these voluminous foams, due to geometrical constrains (bubble volume fraction higher than close packing) with foam films formed between the bubbles.

3.2. Foamability in Kenwood mixer

In this method we measured the temporal evolution of the foam volume upon intensive shearing of the surfactant solution. The experimental results for the lowest and the highest studied concentrations of 0.5 mM and 50 mM of the studied surfactants are compared in Fig. 3. One sees that the kinetics of air entrapment in the Kenwood mixer differs very significantly from that in the Bartsch test. In the Kenwood mixer we observe a well-defined induction period for all studied surfactants, at all studied concentrations. This induction period is related to a relatively slow process of accumulation of a critical volume of bubbles on the solution surface – these bubbles increase the level of the solution surface up to the regions in the mixer where the highest shear rate is realized (the shear rate is significantly lower in the mixer regions situated below and above the optimal one [32]). The rate of air entrapment strongly depends on the local shear rate at the level of the solution/foam surface, because this is the region where the surface waves are generated and the air is entrapped [32].

As seen from Fig. 3, the induction period depends very significantly on the type of surfactant used and its concentration, which reflects the significant differences in the ability of the surfactants to stabilize newly generated bubbles. The induction period is followed by a period of fast air entrapment (when the solution/foam surface is in the high shear-rate region in the mixer) after which the equilibrium foam volume is reached

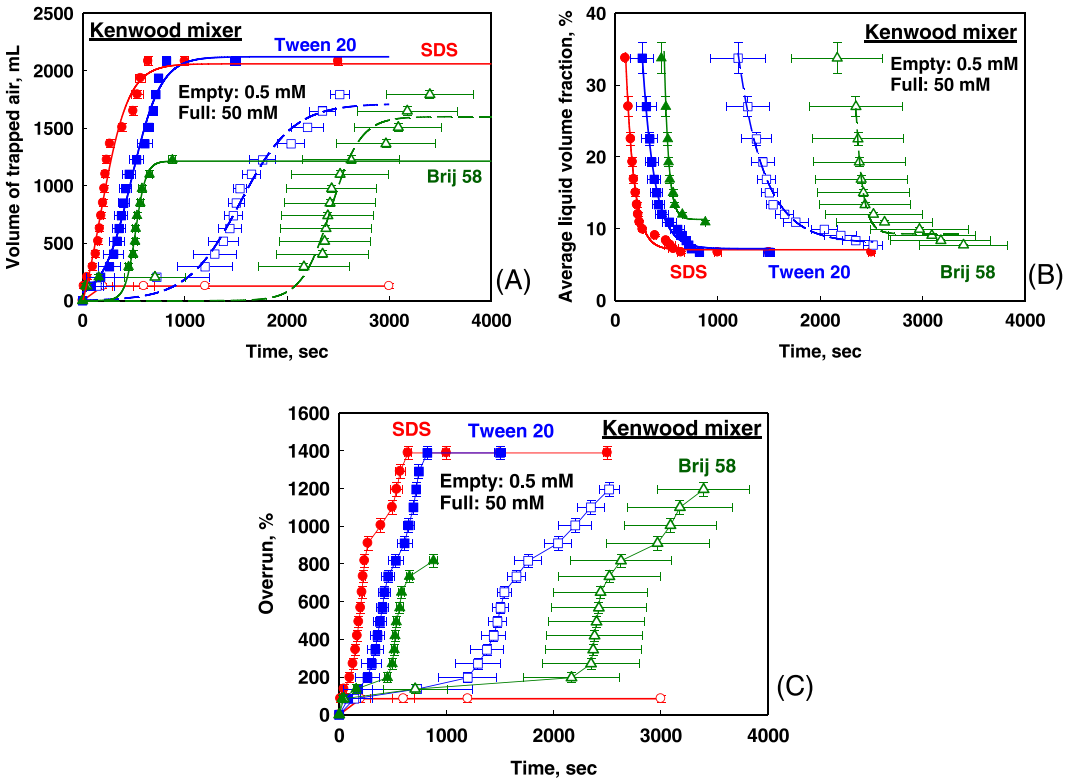

Fig. 3. Foamability in Kenwood mixer: (A) Volume of trapped air; (B) Average liquid volume fraction, and (C) Overrun, as functions of the mixing time for solutions of SDS (red circles), Tween 20 (blue squares) and Brij 58 (green triangles), all solutions studied at 0.5 mM (empty symbols) and 50 mM (full symbols). The symbols show the experimental data, whereas the curves in (A) are the best fits to these data by Eq. (6) and the curves in (B) are the best fits by Eq. (7). The horizontal error bars show the scattering in the time needed to reach a given foam volume in separate experiments. The vertical error bars show the uncertainty in the foam volume measurements. (For interpretation of the references to color in this figure legend, the reader is referred to the web version of this article.)

and the further stirring does not change the volume of the generated foam anymore, Fig. 3A. This is the so called "plateau region" in which the foam volume is determined by the foam rheological properties, as explained in [32].

To characterize the foaming properties of the solutions in this test, we determined the induction time, t_{IND}, the final amount of trapped air, $V_{A\infty}$, and the final average liquid fraction, $\Phi_{L\infty}$. The induction time is determined from the best fit to the experimental data for $\Phi_L(t)$, in the region of moderate and low $\Phi_L < 35\%$, by the following equation:

$$\Phi_L = \Phi_{L\infty} + \Phi_{L1}\exp(-(t-t_{IND})/t_L) \quad \text{at} \quad \Phi_L < 35\ \% \tag{6}$$

This equation describes relatively well the obtained experimental data as seen in Fig. 3B.

The maximal volume of trapped air is determined from the best fit to the experimental data $V_A(t)$ by the following expression:

$$V_A = \frac{V_{A\infty}}{1+\exp(-(t-t_{50\%})/t_A)} \tag{7}$$

where $V_{A\infty}$ is the final foam volume in the plateau region, $t_{50\%}$ is the time required to reach 50% of $V_{A\infty}$, and t_A characterizes the rate of air entrapment at $t = t_{50\%}$ by the expression:

$$\left.\frac{dV_A}{dt}\right|_{t=t_{50\%}} = \frac{V_{A\infty}}{4t_A} \tag{8}$$

Thus, we characterized the foam formation in this test by (1) The maximum volume of entrapped air after very long period of time, $V_{A\infty}$, as determined from the best fit to the experimental data by Eq. (7); (2) The induction time, t_{IND}, defined as the time required to reach air volume fraction of 66% in the foam; (3) The time required to entrap 50% of $V_{A\infty}$ as determined by Eq. (7); (4) The experimentally measured average bubble size in the final foam after stopping the shearing. All these characteristics are shown in Fig. 4, as functions of the surfactant concentration.

Interestingly, we observed that the foam volume passed through a maximum for Brij 58 in this test, as a function of surfactant concentration, see Fig. 4A. Similar results were obtained with another nonionic surfactant Tween 40 (data not shown). For Brij 58 the highest foam volume was reached at 2.5 mM Brij58 and the further increase of surfactant concentration led to significant reduction in the final foam volume. The decrease of the foamability of Brij 58 solutions at high surfactant concentrations was accompanied with a substantial decrease in the mean bubble size in the respective foams, Fig. 4B. As shown in our previous study [32], the amount of entrapped air and the mean bubble size in the forming foam are strongly coupled through the foam rheological properties. The decrease in mean bubble size leads to significant increase of the foam shear stress in the mixer. As a consequence, the air entrapment is suppressed by the higher visco-elasticity of the foam containing smaller bubbles.

In our previous study [32] we showed that the decrease of the mean bubble size and the related lower air entrapment can be caused by higher viscosity and/or by higher dilatational surface modulus of the foamed surfactant solution. To clarify the reason for the observed decreased foam volume and bubble size at high Brij 58 concentrations, we measured the viscosity and the surface dilatational modulus of these solutions. We found that the viscosity of 50 mM Brij 58 is 1.8 mPa s, viz. it is slightly higher than the viscosity of 2 mM Brij 58 (1.0 mPa s). However, this increase is insufficient to explain the observed strong reduction in the foam volume and bubble size [32]. On the other hand, the surface modulus of 50 mM Brij 58 was measured to be very high, ≈ 1000 mN/m, which means that, at high concentrations, this long-chain surfactant forms condensed adsorption layer on the bubble surfaces. As a result, smaller bubbles and suppressed air entrapment are

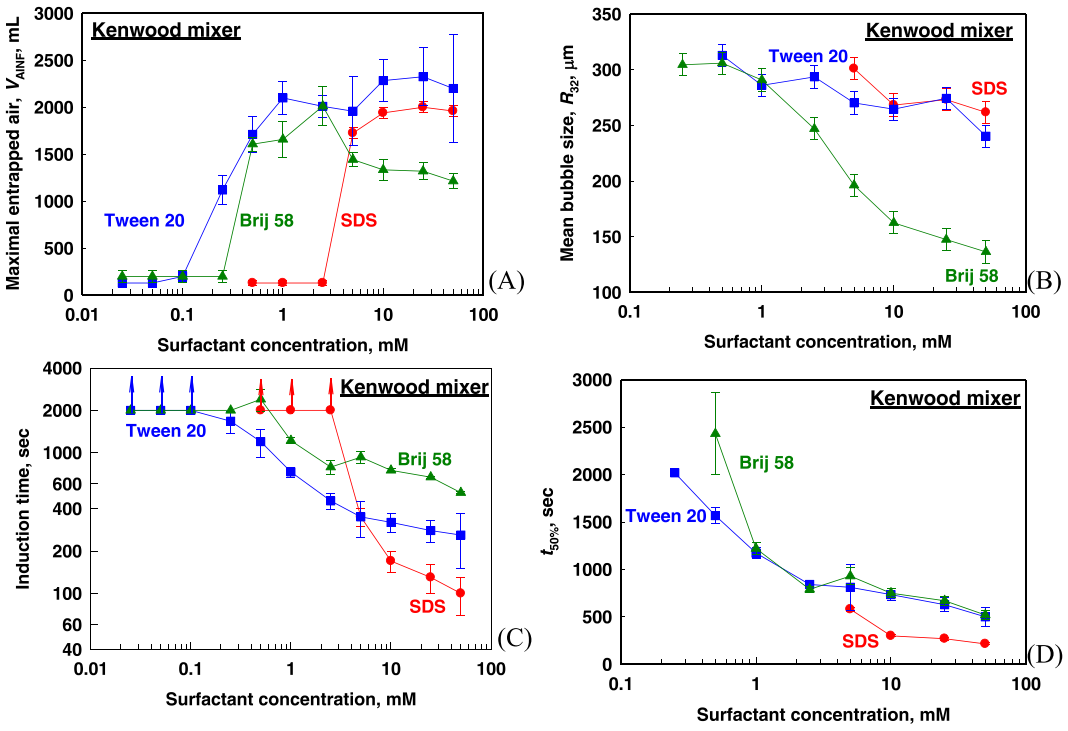

Fig. 4. Foaming in Kenwood mixer: (A) Maximum entrapped air, $V_{A\infty}$; (B) Mean bubble size; (C) Induction time, (D) Time required to reach 50% of $V_{A\infty}$, as functions of surfactant concentration for SDS (red circles), Tween 20 (blue squares) and Brij 58 (green triangles). (For interpretation of the references to color in this figure legend, the reader is referred to the web version of this article.)

observed in the Kenwood mixer. Similar results were obtained with Tween 40 for which the surface modulus also increased with the surfactant concentration.

We conclude from these results that, at high concentrations, the long-chain nonionic surfactants may form condensed adsorption layers on the bubble surface which leads to suppressed foamability and smaller bubbles formed in the Kenwood mixer.

The measured mean bubble sizes were very similar for Tween 20 and SDS solutions at all studied concentrations. The moderate decrease in the mean bubble size with increasing the surfactant concentration is related to the slight increase in the solution viscosity from ca. 0.9 mPa s to 1.4 mPa s for 50 mM Tween 20 and 1.1 mPa s for 50 mM SDS.

The induction time for reaching the average liquid fraction of 33% is shown in Fig. 4C. The induction time is very long at low surfactant concentrations because the formed bubbles are very unstable and rapidly coalesce with each other and with the atmosphere, before forming sufficiently thick layer of bubbles needed to reach the level of high shear rate in the mixer. At high concentrations (> 10 mM) the induction time for the SDS solutions becomes much shorter as compared to the other solutions studied. This means that SDS is more efficient at such concentrations to stabilize the bubbles during the induction period when compared to the nonionic surfactants. Similar conclusion can be drawn when comparing the time required for reaching 50% of the maximal foam volume, Fig. 4D.

3.3. Foaming in the foam rise method (FRM or bubbling test)

During the first 10 s of the experiment in the foam rise method, we

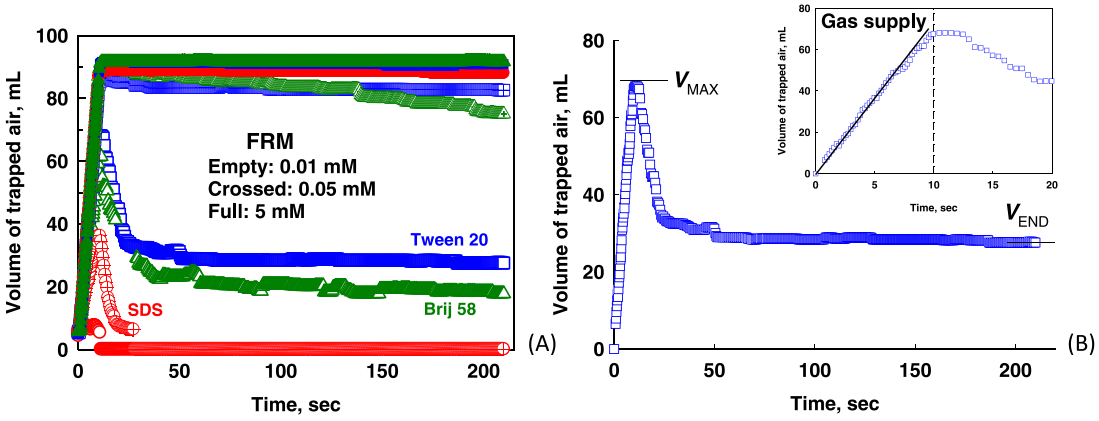

Fig. 5. Foaming in FRM: (A) Volume of trapped air versus time for solutions of the anionic SDS (red circles); the nonionic surfactants Tween 20 (blue squares) and Brij 58 (green triangles) at 0.01 mM (empty symbols); 0.05 mM (crossed symbols) and 5 mM (full symbols); (B) Volume of trapped air versus time for 0.05 mM Tween 20 solution. The maximum entrapped air after 10 s of gas supply, V_{MAX}, and the remaining volume of gas at 200 s after stopping the gas supply, V_{END} are shown. Gas flow rate: 0.6 L/min. (For interpretation of the references to color in this figure legend, the reader is referred to the web version of this article.)

supply gas at fixed flow rate and measure the volume of the trapped air as a function of time. After stopping the gas supply, we monitor the foam decay during the following 200 s to characterize foam stability. The apparatus measures also the bubble size after stopping the foam generation.

These experiments were performed at three gas flow rates: 0.3, 0.6 and 0.9 L/min. Illustrative results for the studied surfactants are shown in Fig. 5. One sees that the foam volume during the gas supply increases almost linearly with time at high surfactant concentrations. At such concentrations, the surfactant adsorbs rapidly and prevents the bubble coalescence – thus, all supplied gas remains trapped in the foam. In contrast, when the surfactant concentration is below a given threshold concentration, the gas bubbles coalesce with the atmosphere upon reaching the solution surface and the volume of the trapped gas is smaller when compared to the total amount of introduced gas, Fig. 5. The bubble coalescence continues even after stopping the gas supply and, therefore, the volume of the trapped air could decrease with time during this second period, depending on the surfactant used and its concentration.

Our attempt to use the approach developed in Ref. [49–51] was unsuccessful because the time for gas supply is very short, 10 s only, from which the first several seconds the liquid fraction is relatively high in the foam and the theoretical models developed in Ref. [49–51] for dry foam cannot be applied. As a consequence, the difference in the initial and final slopes that are required to determine the critical cross section area of the Plateau border for inducing coalescence cannot be determined with sufficient accuracy in our experimental procedure, see the inset in Fig. 5B.

To characterize the ability of the surfactants to stabilize the bubbles during the initial period of gas supply, we determine the volume of trapped gas at the end of the bubbling stage, denoted as V_{MAX}. To characterize the surfactant ability to stabilize the foam during the rest period, we measured the volume of trapped gas after 200 s, denoted as V_{END}, see Fig. 6B.

The experimental results for V_{MAX}, V_{END} and the mean bubble size in the foams formed after 10 s of gas supply are presented in Fig. 6, as functions of surfactant concentration, at the three gas flow rates studied. One sees clearly that the surfactant stabilizes the gas bubbles against coalescence with the atmosphere only above a certain threshold surfactant concentration which depends on the specific surfactant. Interestingly, when considering the foam stabilization during the second stage (after stopping the gas flow), this threshold surfactant concentration is almost the same for Tween 20 and Brij 58 (≈ 0.01 mM) and it is by 30 times higher for SDS (≈ 0.3 mM). In other words, with SDS stable foams are formed at higher surfactant concentrations and the bubbles are smaller when compared to Tween 20 and Brij 58. Note that the constant values of V_{MAX} and V_{END}, reached above certain surfactant concentrations, mean that the whole amount of introduced gas remains stable during the gas supply period if V_{MAX} = const and remains stable even after stopping the gas supply if V_{END} = const.

3.4. Comparison of the results obtained in the three foam tests

In this section we compare the foamability of the studied surfactants in the three foam tests. In general, various measures can be used to compare the foamability, such as the average liquid volume fraction, the overrun, or the relative foam volume. Because the three tests used in the current study are (intentionally) quite different with respect to the mechanism of gas entrapment, we cannot use the average liquid volume fraction and the overrun, because these two quantities are determined mainly by the time for gas supply and the gas flow rate in the FRM – effects which are unrelated to the surfactant adsorption properties.

Therefore, below we present and discuss the relative foam volumes to compare the foamability of the surfactants in the three foam tests. To determine the relative foam volume, we normalize (divide) the volumes of the foams, generated by the various surfactant solutions, by the foam

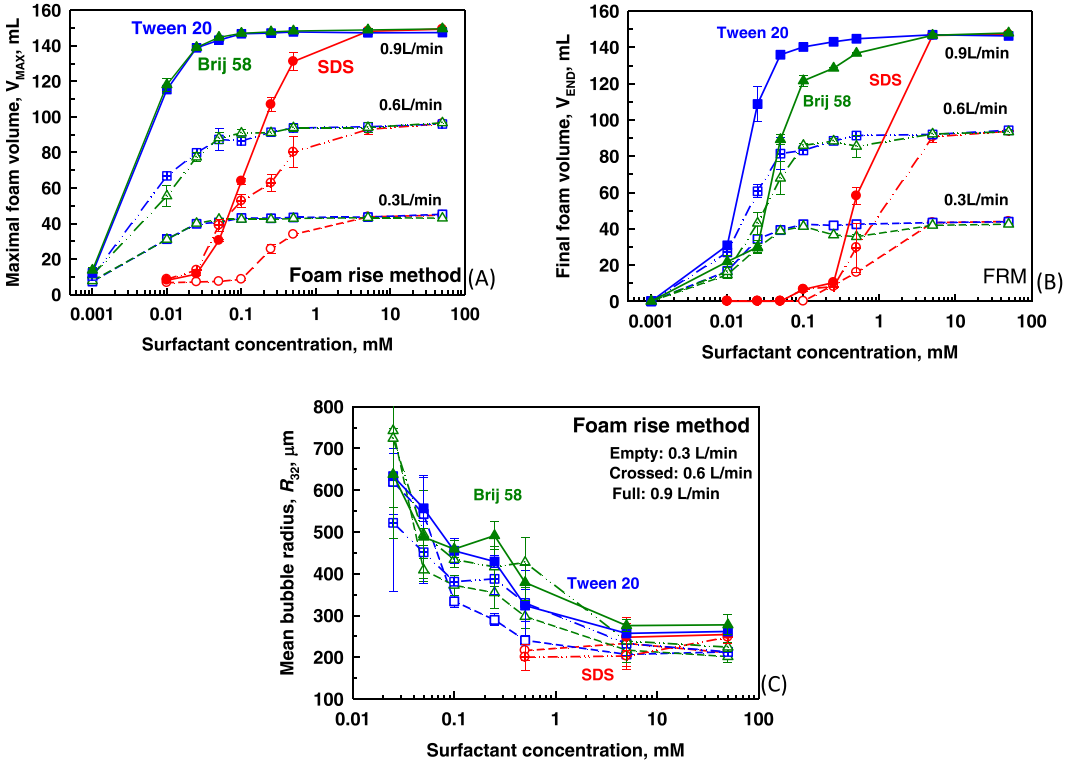

Fig. 6. Foaming Rise Method: (A) Maximum volume of trapped air, V_{MAX}; (B) Final volume of trapped air after 200 s of rest period, V_{END}; (C) Mean bubble radius after 10 s of gas blowing, all as functions of surfactant concentration, for the anionic SDS (red circles) and the nonionic Tween 20 (blue squares) and Brij 58 (green triangles). Gas flow rates: 0.3 L/min (empty symbols); 0.6 L/min (crossed symbols) and 0.9 L/min (full symbols). (For interpretation of the references to color in this figure legend, the reader is referred to the web version of this article.)

volume for a reference surfactant solution in the respective foaming test. This approach has the advantage to be directly extendable to other foaming tests and surfactants.

We selected 50 mM SDS as a reference surfactant solution, because its foamability is very high in all three foaming tests studied. The volume of air entrapped in 50 mM SDS is 120 mL in the Bartsch test; 2270 mL in the Kenwood mixer; and 45 mL at 0.3 L/min, 96 mL at 0.6 L/min, and 149 mL at 0.9 L/min in the FRM. These values are used below to determine the relative foamability of all other surfactant solutions in the various tests.

The results for the relative foamability, as a function of surfactant concentration, are compared in Fig. 7. For all surfactants in all foam tests we see a well-defined threshold surfactant concentration, above which the foamability increases rapidly. For a given surfactant, this threshold concentration depends strongly on the foam test used – it is the lowest when the foam is generated in the FRM, intermediate in the Kenwood mixer, and the highest in the Bartsch test. This order is explained by the different times allowed for surfactant adsorption on the bubble surfaces in the various tests, as explained below.

In the *Bartsch test* the rate of air entrapment is very fast and the bubble surfaces have very short time (fraction of a second) to be covered by surfactant before colliding with other bubbles, Fig. 1C. Furthermore, the bubbles in the Bartsch test are subject to very strong hydrodynamic stresses, created by the inertial forces in the shaken liquid, which strongly deform the bubbles and increase their surface area in the process of bubble collisions.

In our previous study [38] we found that the volume of the foam formed in the *Bartsch test* correlates well with the dynamic surface tension and with the surface coverage of the bubbles, $\theta(\tau) = \Gamma(\tau)/\Gamma_{CMC}$, where $\Gamma(\tau)$ is the dynamic adsorption after time τ of surface generation and Γ_{CMC} is the equilibrium surfactant adsorption at CMC. For details see the explanations in Ref. [38]. We showed also that the characteristic time for surfactant adsorption on the bubble surface, before colliding with other bubbles, is $\tau_{BT} \approx 0.4$ s in this test. To account for the surface area expansion explained in the previous paragraph, we determined the properties of the dynamic adsorption layers formed at 0.4 s period in the maximum bubble pressure method (MBPM), in which the bubbles rapidly expand their surface area, similarly to the colliding bubbles in the Bartsch test. As explained in Ref. [38], this period of 0.4 s with expanding bubble surface corresponds to ≈ 10 ms of the so-called "universal surface age", characterizing the kinetics of adsorption from the same surfactant solution on non-expanding solution surface. This comparison shows that it is extremely important to distinguish between the adsorption onto expanding solution surface from that onto non-expanding one.

In the *FRM*, the gas is supplied from the bottom of the surfactant solution and the bubbles have a certain period of time to float up through the surfactant solution before reaching the air-water interface where they could coalesce with the atmosphere and/or with other bubbles, Fig. 1A. In this test, the bubbles travel through the solution and collide with the other bubbles at almost fixed surface area, because the hydrodynamic forces are relatively mild when compared to bubble capillary pressure – only the buoyancy is driving the bubble motion and collisions. From this viewpoint, the FRM is very different from the Bartsch test and this difference should be taken into account when defining the method for characterizing the dynamic adsorption layers on the bubble surfaces in the FRM.

After reaching the surface of the surfactant solution in the FRM, the bubble could stay stable, coalesce with other bubbles, or coalesce with the atmosphere. Only the coalescence of the uppermost layer of bubbles with the atmosphere reduces the volume of trapped air, see Movie 1. The bubble-bubble coalescence increases the mean bubble size but does not reduce the total volume of trapped air. In our FRM, the time for the first bubbles to come in contact with the solution-air interface was ≈ 0.3 s, as observed with a high speed camera. However, the bubbles arriving at the air-water interface did not coalesce immediately with the atmosphere, because the formed foam films needed additional time to thin down to their critical thickness for rupture. During this period, additional surfactant adsorbs on the bubble surface and newly generated bubbles arrive from the bottom, coming in contact with the bubbles that had

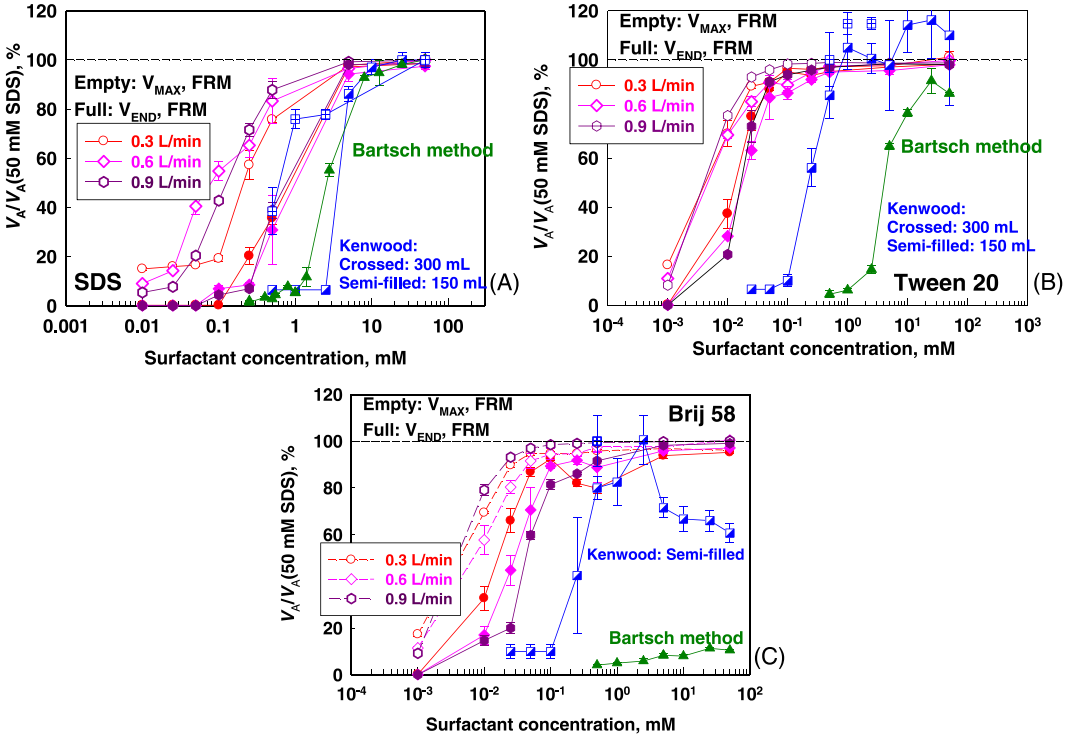

Fig. 7. Relative amount of entrapped air, as a function of surfactant concentration, for foams stabilized by (A) SDS; (B) Tween 20, and (C) Brij 58, in the three foam tests as noted in the figures.

previously arrived. Except for the lowest surfactant concentrations, the rate of bubble supply was faster than the rate of bubble coalescence with the atmosphere and, therefore, the foam volume increased during the stage of gas supply. After stopping the gas supply, the bubble coalescence continued and the foam volume decreased until reaching the final foam volume, as shown in Fig. 5B. The characteristic time for reaching the final foam volume after stopping the gas supply varied between 2 and 100 s, depending on the specific surfactant system and the gas flow rate. The exception are the foams formed from 0.5 mM SDS solution at the three studied flow rates and the foam formed from 0.25 mM SDS solution at 0.3 L/min flow rate. These foams did not reach their steady volume even 200 s after stopping the gas supply – they continued to decay. All these observations show that an adequate characteristic time for surfactant adsorption in this test is somewhere between 10 and 100 s. Therefore, in the following estimates we used the dynamic surface tension measured 50 s after creating the solution surface in the Wilhelmy plate method, i.e. the characteristic time for the FRM was defined as $\tau_{FRM} \approx 50$ s (for adsorption on non-expandable surface). Note that due to the slow adsorption of some of the components in the used surfactants, the measured surface tension were close to, but not exactly equal to the equilibrium surface tensions. Numerical checks showed that the exact value of τ_{FRM} was not very significant – all conclusions of the current study would remain the same, provided that τ_{FRM} was taken in the justified range between 10 s and 100 s

In the *Kenwood mixer*, the bubbles are first entrapped at the solution-air interface and should stay stable during the induction period to build a rising foam layer, Fig. 1B. Note that the bubbles are subject to strong shear forces in the mixer after their formation, which means that the bubbles deform and their surface area varies in this test. Therefore, we conclude that the time scale for bubble formation in the Kenwood mixer should be comparable to the duration of the induction period, viz. ≈ 15 s surface age, as determined in the MBPM, because the bubble surface is expanding in the mixer due to the shear forces.

Following the above arguments, in Fig. 8 we compare the relative foamability as a function of the dynamic surface tension and of the surface coverage, $\theta = \Gamma(\tau)/\Gamma_{CMC}$, calculated at the characteristic timescales of $\tau_{BT} = 0.4$ ms for the Bartsch test and $\tau_{KM} = 15$ s for the Kenwood mixer (both determined by the MBPM), and $\tau_{FRM} = 50$ s for the FRM (bubbling test), as determined by the Wilhelmy plate method. To calculate the values of $\Gamma(\tau)$ and Γ_{CMC} we used the approach described in Section 4 in Ref. [38] and the data for the equilibrium and dynamic surface tensions of the respective surfactant solutions. More precisely, we determined the values of Γ_{CMC} from the fit to the equilibrium surface tension isotherms by Eqs. (1) and (4) in Ref. [38] for the nonionic surfactants and by Eqs. (10) and (11) in Ref. [38] for the ionic surfactant. The values of $\Gamma(\tau)$ were determined from the fit to the dynamic surface tension data, measured by the MBPM or by the Wilhelmy plate method, as explained above, using Eq. (14) in Ref. [38].

One sees in Fig. 8a relatively good agreement between the results, obtained in the different foam tests for a given surfactant. Larger deviation from the master curves for both the ionic and nonionic surfactants is observed only for the foams formed in the FRM at surfactant concentrations around the threshold concentration (the symbols above the curves at $\Gamma/\Gamma_{CMC} \approx 0.2$). These deviations are most probably due to the fact that, under these conditions, the time allowed for surfactant adsorption in this foam test is longer than 50 s, because the foam destruction continues up to 200 s after stopping the gas supply - during all this period, the adsorption on the bubble surface still continues and the surface coverage in the foam gets higher than the one calculated for 50 s adsorption time.

Besides the obvious difference between the ionic and nonionic surfactants in Fig. 8 (see also Ref. [38]), we observed that the surface coverage which ensures the stabilization of foam is > 0.98 for Brij 58, whereas for Tween 20 the threshold surface coverage is slightly lower, ≈ 0.90. The surfactant Brij 35 behaves very similarly to Brij 58 in this plot, Fig. 8. The most probable reason for the difference between Tween 20, on one side, and Brij 58 and Brij 35, on the other side, is the occurrence of weak electrostatic repulsion in the solutions of Tween 20. Indeed, we observed that foam films stabilized by Tween 20 are thicker than those for the other non-ionic surfactants and the film thickness decreases when NaCl is added to the surfactant solutions, thus indicating the presence of weak electrostatic repulsion between the foam film surfaces, see Fig. 9. Note that electrostatic forces were reported previously for solutions of another sugar-based nonionic surfactant (alkylpolyglucoside, APG) and were explained with the adsorption of hydroxyl OH^- ions on the air-water interface [52] (and possibly on the sugar groups of these surfactants), due to the formation of strong hydrogen bonds.

One can make a step further in this analysis and try to explain the threshold surfactant concentrations, C_{TR}, at which the foamability of the respective solution increases rapidly in the given method. From the results shown in Fig. 7 we can determine C_{TR}, defined as the concentration at which the foamability of the respective solution reaches 75% of the maximal foamability in the given method. The values of C_{TR} determined in this way are compared in Fig. 10.

In the FRM, $C_{TR} \approx 0.3$ mM for SDS during the period of gas supply and about 2.3 mM after stopping the gas supply. For comparison, the CMC of SDS is ≈ 8 mM. For the nonionic surfactants, C_{TR} in the FRM is much lower: $C_{TR} \approx 0.03$ mM for Tween 20 and $C_{TR} \approx 0.06$ mM for Brij 58, based on the results for the final foam volume in the rest period, and $C_{TR} \approx 0.012$ mM for both nonionic surfactants in the gas supply period. Note that the latter value is close to CMC for Tween 20 and around 4

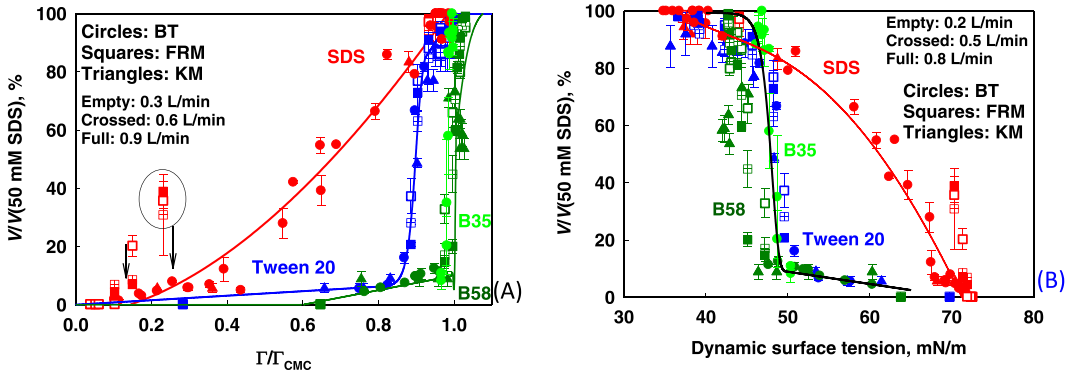

Fig. 8. Relative foamability as a function of (A) the surface coverage, Γ/Γ_{CMC}, and (B) dynamic surface tension for the foams formed in different foam tests and stabilized by four surfactants (SDS, Tween 20, Brij 58 and Brij 35). The surface coverage is determined by using the values of the dynamic surface tension measured after 0.4 s for the Bartsch test and 15 s for Kenwood mixer (measured by MBPM) and after 50 s for the FRM (measured by Wilhelmy plate method). The black arrows indicate two solutions of SDS of low concentration (0.25 and 0.5 mM) for which the foam in the FRM did not reach its steady volume (the foam still decays) even 200 s after stopping the gas supply.

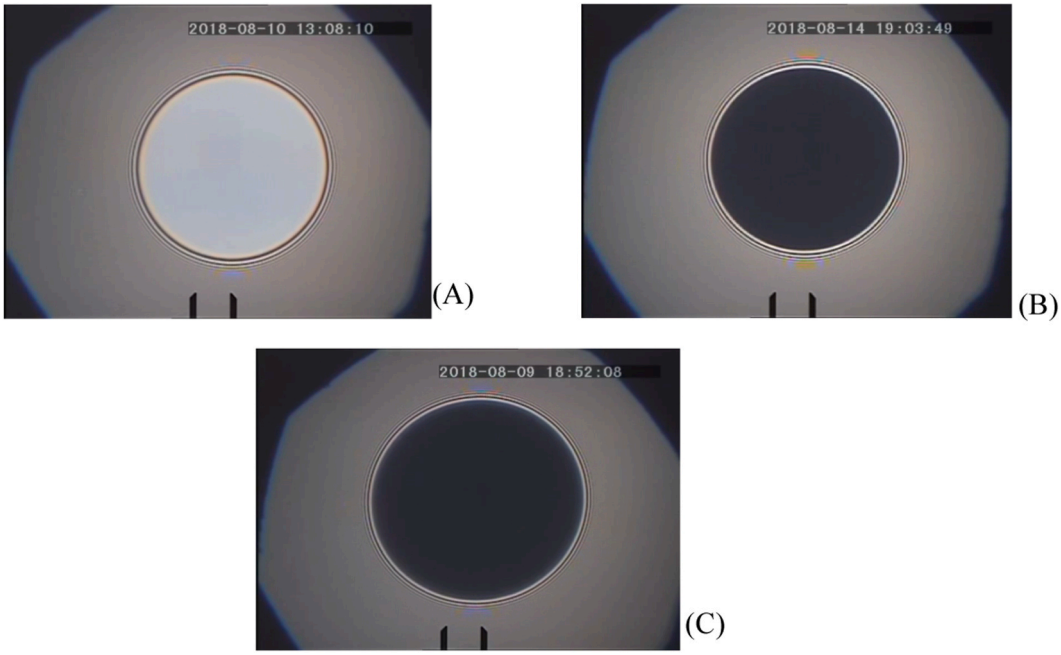

Fig. 9. Illustrative images of the foam films formed from 5 mM surfactant solution of (A) Tween 20; (B) Brij 35, and (C) Tween 20 + 10 mM NaCl. Note the bright appearance of the foam film in (A) which has a thickness of ≈ 55 ± 5 nm, whereas the other two foam films are much thinner, in the range of 15–20 nm.

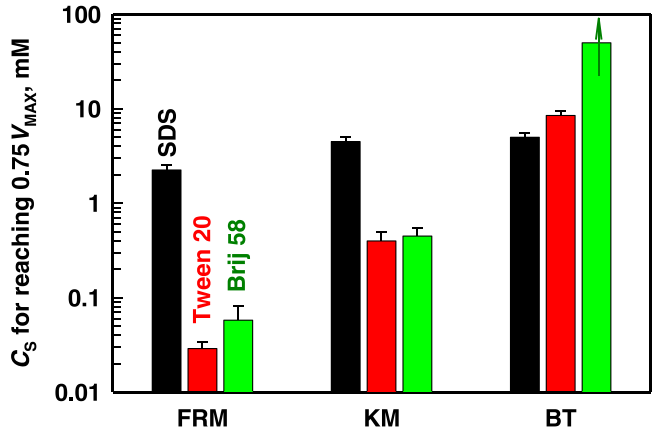

Fig. 10. Threshold surfactant concentration, C_{TR}, required to reach 75% of the maximum volume of entrapped air in the different experimental test for foams stabilized by SDS (black bars), Tween 20 (red bars) and Brij 58 (green bars). FRM denotes the foam rise method, KM – Kenwood mixer, and BT – Bartsch test. (For interpretation of the references to color in this figure legend, the reader is referred to the web version of this article.)

times higher than CMC for Brij 58.

In the Kenwood mixer $C_{TR} \approx 4.5$ mM for SDS, ≈ 0.4 mM for Tween 20, and ≈ 0.45 mM for Brij 58.

The highest values of C_{TR} for all studied surfactants are determined in the Bartsch test: ≈ 5 mM for SDS; ≈ 8.5 mM for Tween 20 and > 50 mM for Brij 58.

The above results reinforce the conclusion from our previous study [38] that the CMC cannot be used as a predictor of the threshold surfactant concentration at which the foaming increases and the foam becomes stable. For example, foam stabilization was observed at 0.5 ×CMC for SDS, 33 × CMC for Tween 20, and 150 × CMC for Brij 58 in the Kenwood mixer.

Following an approach developed originally for emulsions [53,54], we can try to predict the value of C_{TR} for the nonionic surfactants in the slow-foaming tests (FRM and Kenwood mixer) by calculating the necessary surfactant concentration required to cover completely the surfaces of the bubbles, formed during foaming. For this purpose we can modify the surfactant mass-balance equation derived in Ref. [53,54] to obtain:

$$C_{TR} = \frac{6(1-\Phi_L)\theta_{TR}\Gamma_{CMC}}{\Phi_L d_{32}} + CMC \quad (9)$$

Here θ_{TR} is the threshold surface coverage which is ≈ 0.95 ± 0.05 for the nonionic surfactants (see Fig. 8), Γ_{CMC} is the surfactant adsorption at CMC (≈ 3.0 μmol/m^2 for Brij 58 and ≈ 3.6 μmol/m^2 for Tween 20) [38]. The CMC is ≈ 0.003 mM and ≈ 0.012 mM for Brij 58 and Tween 20, respectively [38]. Φ_L is the characteristic average liquid volume fraction for the given foam test, corresponding to ca. 75% foam volume from that formed with 50 mM SDS solution, and d_{32} is the mean bubble diameter. We can assume for the following approximate estimates that the mean bubble size at C_{TR} is close to that in the stable foams from 50 mM SDS solution – this assumption is justified for the foamed solutions with low viscosity (ca. 1 mPa s), similar surface tension (ca. between 25 and 35 mN/m) and low surface modulus (below ca. 50 mN/m).

In the Kenwood mixer, the average liquid volume fraction in the final foam produced from 50 mM SDS solution is 6.6%, which means that at 75% foam volume it is $\Phi_L \approx 8.8\%$. For the other slow-foaming method, the FRM, the mean liquid volume fraction for 50 mM SDS solution is 34% for the flow rate of 0.6 L/min, which means that at 75% foam volume it is $\Phi_L \approx 45\%$. The mean bubble size in both methods is d_{32} ≈ 500 μm. Substituting these values in Eq. (9) we estimate the threshold concentrations, which are compared with the experimentally

Table 1
Measured and predicted threshold surfactant concentration by Eq. (9) for Brij 58 and Tween 20 stabilized foams, formed in Kenwood mixer and in the foam rise method at 0.6 L/min gas supply.

Surfactant	C_{TR}, mM			
	Kenwood mixer		Foam rise method	
	Predicted	Measured	Predicted	Measured
Tween 20	0.41	0.40	0.060	0.036
Brij 58	0.37	0.45	0.046	0.056

determined ones in Table 1. One sees that Eq. (9) predicts the threshold surfactant concentrations with a precision better than 15% for the Kenwood mixer and FRM, because the time allowed for surfactant adsorption in this test is sufficiently long to ensure a complete surface coverage of the bubbles by the surfactant available in the foaming solution. For Tween 20 in the FRM the agreement is still reasonable, although being worse than all other systems, probably because of some possible contribution of the weak electrostatic interactions explained above. We can conclude from the comparison shown in Table 1 that the surface coverage is close to the equilibrium one for the nonionic surfactants in the slowly foaming methods, such as the Kenwood mixer and the FRM.

The attempt to apply the same approach to the fast-foaming method, the Bartsch test, led to large discrepancy. The average liquid volume fraction for 50 mM SDS solution in the Bartsch test is 7.7%, which means that the respective liquid fraction at 75% foam volume is $\Phi_L \approx 10\%$. The mean bubble size is $d_{32} = 1$ mm. Substituting these values in Eq. (9) we estimate $C_{TR} \approx 0.165$ mM for Brij 58 and $C_{TR} \approx 0.21$ mM for Tween 20 in this test. Both values are by orders of magnitude lower than the threshold concentrations determined experimentally (8.5 mM for Tween 20 and $>$ 50 mM for Brij 58). Therefore, Eq. (9) cannot be used for prediction of C_{TR} in the fast-foaming methods, because the surfactants have no time to reach their equilibrium adsorption, as the bubbles coalesce before that. This approach cannot be used for ionic surfactants as well, as shown previously with emulsions [53], because the electrostatic interactions change the conditions for bubble/drop stabilization.

Finally, we compare the kinetics of air entrapment in the Bartsch test and in the Kenwood mixer by determining the time required to entrap 50% of V_{MAX} (i.e. the time required to reach 60 mL entrapped air in the Bartsch test and 1135 mL in the Kenwood mixer), see Fig. S1 in the Supplementary Materials. To compare the rate of foam formation for the various surfactants in these two foam tests, we scale the data shown in Fig. S1 by dividing the time required to entrap 50% of V_{MAX} with 50 mM SDS solution, viz. by 220 s in the Kenwood mixer and by 4.3 shaking cycles in the Bartsch test. The scaled results are shown in Fig. 11. One sees that the relative time for foaming in the Kenwood mixer is shorter than that in the Bartsch test for both nonionic surfactants, which is related to the longer time for surfactant adsorption in the Kenwood mixer. The difference between these two foam tests is particularly large at concentrations around C_{TR}, because the kinetic effects are most important around this concentration. The relative time for air entrapment at high surfactant concentrations $C_S > C_{TR}$ is shorter for SDS in both methods which is explained by the strong electrostatic stabilization of the bubbles in SDS solutions.

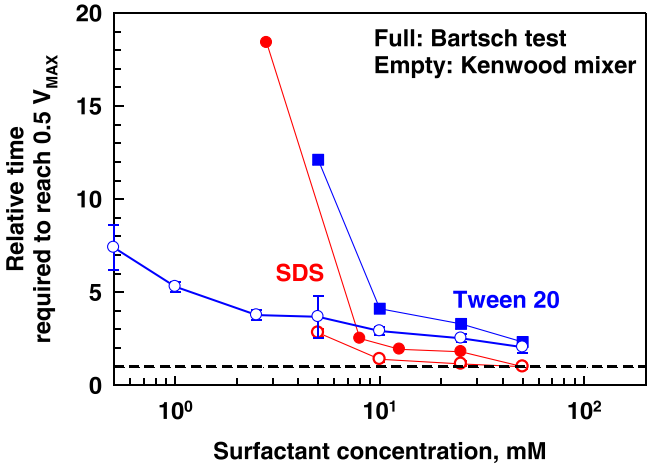

Fig. 11. Relative time to reach 50% of V_{MAX} as a function of surfactant concentration for foams formed in the Bartsch test (full symbols) and in Kenwood mixer (empty points).

4. Conclusions

Systematic experiments are performed for comparing the foamability of one anionic (SDS) and two nonionic surfactants (Tween 20 and Brij 58), at surfactant concentrations varied between 10^{-3} and 50 mM, in three foaming tests which differ very significantly in the hydrodynamics of the foaming process. The obtained results are analysed from the viewpoints of the rate of surfactant adsorption and the hydrodynamic conditions during foaming.

The main conclusions could be summarized as follows:

(1) For all studied surfactants in all foam tests we observe a well-defined threshold surfactant concentration, C_{TR}, above which the foamability increases steeply and soon afterwards it reaches the maximum foam volume for the given test.

(2) C_{TR} depends strongly on the dynamics of the foaming process: it is the lowest in the FRM, intermediate in the Kenwood mixer, and much higher in the Bartsch test. The values of C_{TR} in the "slow-foaming" tests (Foam rise method - FRM and Kenwood mixer) are much lower for the nonionic surfactants when compared to the anionic one. In contrast, C_{TR} is the lowest for the anionic SDS in the "fast-foaming" Bartsch test.

(3) The analysis of the hydrodynamic conditions during foaming shows that the relevant time-scales for surfactant adsorption are very different in the tests studied. The adsorption in the FRM occurs for seconds on almost fixed surface area of the bubbles. In contrast, the bubble surface is rapidly expanding and the bubble-bubble collisions appear very soon after the bubble formation in the Bartsch test. In the Kenwood mixer we have sheared bubbles, also with deforming surfaces, but the time-scale is much longer than in the Bartsch test. These differences in the bubble dynamics during foaming could be captured by assigning relevant time-scale for each test and accounting for the bubble expansion in the Bartsch test and in Kenwood mixer: $\tau_{BT} \approx 0.4$ s for the Bartsch test and $\tau_{KM} \approx 15$ s for the Kenwood mixer, as measured by the MBPM (expanding surface area), and $\tau_{FRM} \approx 50$ s for the FRM (bubbling test), as measured by the Wilhelmy plate method (fixed surface area).

(4) All data for the relative foamability are described by two master curves for the ionic and nonionic surfactants, respectively, when plotted as a function of the bubble surface coverage, Fig. 8A. For the anionic surfactants the relative foamability starts to increase at a surface coverage $\theta \approx 0.2$, whereas a surface coverage of $\theta \approx 0.95 \pm 0.05$ for the nonionic surfactants. This difference is related to the contribution of the electrostatic repulsion, which is very pronounced for the anionic surfactants and weak (Tween 20) or negligible (Brij 58 and Brij 35) for the nonionic ones.

(5) The results show that the slow-foaming methods (FRM and Kenwood mixer) are suitable for preparing foams stabilized by slowly adsorbing surfactants, such as the nonionic Tween 20, Brij 58 and Brij 35, whereas the fast-foaming method (Bartsch test) is more appropriate for foam generation from solutions of rapidly adsorbing surfactants, such as the anionic SDS.

This new approach allowed us for first time to rationalize and compare the results obtained with different surfactants in different foam tests. This comparison became possible by accounting for the differences in the characteristic times of the different foam tests and their comparison with the characteristic times of surfactant adsorption, which depend on both the surfactant type and surfactant concentration. The performed analysis is based on clear physicochemical understanding and description of the governing dynamic processes during foaming. Therefore, the main conclusions and the approaches for data interpretation are expected to be applicable for wide range of systems, although the characteristic times of each specific foam test could vary, depending on the test type and the specific hydrodynamic conditions (flow rate,

rotation speed, frequency and amplitude of oscillations, etc.). One could expect future studies to expand and deepen this approach to a variety of other foam tests and surfactant systems.

CRediT authorship contribution statement

Borislava Petkova: Investigation, Formal analysis, Visualization, Writing – Original draft. **Slavka Tcholakova**: Conceptualization, Methodology, Formal analysis, Writing – Review&Editing, Supervision. **Nikolai Denkov**: Conceptualization, Methodology, Writing – Review&Editing.

Declaration of Competing Interest

The authors declare that they have no known competing financial interests or personal relationships that could have appeared to influence the work reported in this paper.

Acknowledgment

The authors thank Mrs. Mila Temelska and Mrs. Dora Dimitrova, both from Sofia University, for their help in surface tension measurements. This work was partially supported by the European Regional Development Fund within the Operational Programme "Science and Education for Smart Growth 2014 - 2020" under the Project CoE "National center of mechatronics and clean technologies" BG05M2OP001-1.001-0008".

Appendix A. Supporting information

Supplementary data associated with this article can be found in the online version at doi:10.1016/j.colsurfa.2021.127009.

References

[1] Y.S. Cho, J.S. Laskowski, Effect of flotation frothers on bubble size and foam stability, Int. J. Miner. Process. 64 (2–3) (2002) 69–80, https://doi.org/10.1016/S0301-7516(01)00064-3.
[2] J. Wang, A.V. Nguyen, S. Farrokhpay, A critical review of the growth, drainage and collapse of foams, Adv. Colloid Interface Sci. 228 (2016) 55–70, https://doi.org/10.1016/j.cis.2015.11.009.
[3] N. Barbian, K. Hadler, E. Ventura-Medina, J.J. Cilliers, The froth stability column: linking froth stability and flotation performance, Miner. Eng. 18 (3) (2005) 317–324, https://doi.org/10.1016/j.mineng.2004.06.010.
[4] S.J. Neethling, H.T. Lee, J.J. Cilliers, Simple relationships for predicting the recovery of liquid from flowing foams and froths, Miner. Eng. 16 (11) (2003) 1123–1130, https://doi.org/10.1016/j.mineng.2003.06.014.
[5] K. Hadler, J.J. Cilliers, The effect of particles on surface tension and flotation froth stability, Min. Metall. Explor. 36 (2019) 63–69, https://doi.org/10.1007/s42461-018-0020-z.
[6] Ashiwani Kumar Gupta, P.K. Banerjee, Arun Mishra, P. Satish, Pradip, Effect of alcohol and polyglycol ether frothers on foam stability, bubble size and coal flotation, Int. J. Miner. Process. 82 (3) (2007) 126–137, https://doi.org/10.1016/j.minpro.2006.09.002.
[7] E. Allen Foegeding, P.J. Luck, J.P. Davis, Factors determining the physical properties of protein foams, Food Hydrocoll. 20 (2–3) (2006) 284–292, https://doi.org/10.1016/j.foodhyd.2005.03.014.
[8] M. Hammershøj, A. Prins, K.B. Qvist, Influence of pH on surface properties of aqueous egg albumen solutions in relation to foaming behavior, J. Sci. Food Agric. 79 (6) (1999) 859–868, https://doi.org/10.1002/(SICI)1097-0010(19990501)79:6<859::AID-JSFA301>3.0.CO;2-C.
[9] M.V. Tzoumaki, D. Karefyllakis, T. Moschakis, C.G. Biliaderis, E. Scholten, Aqueous foams stabilized by chitin nanocrystals, Soft Matter 11 (31) (2015) 6245–6253, https://doi.org/10.1039/c5sm00720h.
[10] E. Yalçın, S. Çelik, E. İbanoğlu, Effects of irradiation on protein electrophoretic properties, water absorption and cooking quality of lentils, Int. J. Food Sci. Nutr. 55 (2004) 641–648, https://doi.org/10.1007/s00217-007-0618-8.
[11] Dengfeng Peng, Weiping Jin, Cuie Tang, Ying Lu, Wenqiang Wang, Jing Li, Bin Li, Foaming and surface properties of gliadin nanoparticles: influence of pH and heating temperature, Food Hydrocoll. 77 (2018) 107–116, https://doi.org/10.1016/j.foodhyd.2017.09.026.
[12] George C. Sawicki, Impact of surfactant composition and surfactant structure on foam control performance, Colloids Surf. A Physicochem. Eng. Asp. 263 (1–3) (2005) 226–232, https://doi.org/10.1016/j.colsurfa.2004.12.026.
[13] R. Arun Karthick, Ketan Jangir, Pradipta Chattopadhyay, Foaming and cleaning performance comparison of liquid detergent formulations using mixtures of anionic and nonionic surfactants, Tenside Surfactants Deterg. 55 (2) (2018) 162–168, https://doi.org/10.3139/113.110553.
[14] A.G. Deshmukh, B.B. Gogte, Foaming and stain removing laundry liquid detergents based on novel polymer and sorbitol, Int. J. Chem. Sci. 12 (3) (2014) 933–940.
[15] Nafsika Ganidi, Sean Tyrrel, Elise Cartmell, Anaerobic digestion foaming causes – a review, Bioresour. Technol. 100 (23) (2009) 5546–5554, https://doi.org/10.1016/j.biortech.2009.06.024.
[16] Mao-Sung Yeh, Yu-Hong Wei, Jo-Shu Chang, Bioreactor design for enhanced carrier-assisted surfactin production with Bacillus subtilis, Process Biochem. 41 (8) (2006) 1799–1805, https://doi.org/10.1016/j.procbio.2006.03.027.
[17] L. Moeller, A. Zehnsdorf, Process upsets in a full-scale anaerobic digestion bioreactor: over-acidification and foam formation during biogas production, Energy Sustain. Soc. 6 (2016) 30, https://doi.org/10.1186/s13705-016-0095-7.
[18] J.J. Bikerman, Measurement of Foaminess. Foams, Springer-Verlag, New York, 1973, pp. 65–97.
[19] D. Exerowa, P.M. Kruglyakov, Foams and Foam Films: Theory Experiment, Application, Elsevier, Amsterdam, 1998.
[20] I. Cantat, et al., Foams: Structure and Dynamics, Oxford University Press, UK, 2013.
[21] R.K. Prud'homme, S.A. Khan, Foams: Theory, Measurements, and Applications, Marcel Dekker, New York, 1996.
[22] Enda Carey, Cosima Stubenrauch, Foaming properties of mixtures of a non-ionic (C12DMPO) and an ionic surfactant (C12TAB), J. Colloid Interface Sci. 346 (2010) 414–423, https://doi.org/10.1016/j.jcis.2010.03.013.
[23] D. Kawale, A.T. van Nimwegen, L.M. Portela, M.A. van Dijk, R.A.W.M. Henkes, The relation between the dynamic surface tension and the foaming behaviour in a sparger setup, Colloids Surf. A Physicochem. Eng. Asp. 481 (2015) 328–336, https://doi.org/10.1016/j.colsurfa.2015.05.028.
[24] N.D. Denkov, Mechanisms of foam destruction by oil-based antifoams, Langmuir 20 (2004) 9463–9505, https://doi.org/10.1021/la049676o.
[25] Davide Beneventi, Bruno Carre, Alessandro Gandini, Role of surfactant structure on surface and foaming properties, Colloids Surf. A Physicochem. Eng. Asp. 189 (1–3) (2001) 65–73, https://doi.org/10.1016/S0927-7757(01)00602-1.
[26] C.D. Dushkin, T.L. Stoichev, T.S. Horozov, A. Mehreteab, G. Broze, Dynamics of foams of ethoxylated ionic surfactant in the presence of micelles and multivalent ions, Colloid Polym. Sci. 281 (2) (2003) 130–142, https://doi.org/10.1007/s00396-002-0678-z.
[27] Carlos Jimenez-Junca, Alexander Sher, Jean-Claude Gumy, K. Niranjan, Production of milk foams by steam injection: the effects of steam pressure and nozzle design, J. Food Eng. 166 (2015) 247–254, https://doi.org/10.1016/j.jfoodeng.2015.05.035.
[28] S. Silva, A. Espiga, K. Niranjan, S. Livings, J.C. Gumy, A. Sher, Formation and stability of milk foams, in: G.M. Campbell, M.G. Scanlon, D.L. Pyle (Eds.), Bubbles in Food 2: Novelty, Health and Luxury, AACC International, St. Paul, Minnesota, 2008, pp. 153–161.
[29] J. Goh, O. Kravchuk, H.C. Deeth, Comparison of mechanical agitation, steam injection and air bubbling for foaming milk of different types, Milchwissenschaft 64 (2) (2009) 121–124.
[30] A.K.S. Chesterton, G.D. Moggridge, P.A. Sadd, D.I. Wilson, Modelling of shear rate distribution in two planetary mixtures for studying development of cake batter structure, J. Food Eng. 105 (2) (2011) 343–350, https://doi.org/10.1016/j.jfoodeng.2011.02.044.
[31] I. Lesov, S. Tcholakova, N. Denkov, Factors controlling the formation and stability of foams used as precursors of porous materials, J. Colloid Interface Sci. 426 (2014) 9–21, https://doi.org/10.1016/j.jcis.2014.03.067.
[32] Nadya Politova, Slavka Tcholakova, Zhulieta Valkova, Konstantin Golemanov, Nikolai D. Denkov, Self-regulation of foam volume and bubble size during foaming via shear mixing, Colloids Surf. A 539 (2018) 18–28, https://doi.org/10.1016/j.colsurfa.2017.12.006.
[33] W. Hanselmann, E. Windhab, Flow characteristics and modelling of foam generation in a continuous rotor/stator mixer, J. Food Eng. 38 (4) (1998) 393–405, https://doi.org/10.1016/S0260-8774(98)00129-0.
[34] A.B.J. Kroezen, J. Groot Wassink, E. Bertlein, Foam generation in a rotor-stator mixer, Chem. Eng. Process. 24 (3) (1988) 145–156, https://doi.org/10.1016/0255-2701(88)80018-7.
[35] R. Singh, K.K. Mohanty, A simple, efficient, and eco-friendly method for the preparation of 3-substituted-2,3-dihydroquinazolin-4(1H)-one derivatives, Molecules 24 (2019), https://doi.org/10.2118/170942-PA.
[36] O. Bartsch, Über Schaumsysteme, Kolloidchem. Beih. 20 (1–5) (1924) 1–49, https://doi.org/10.1007/BF02558490.
[37] Jongju Lee, Alex Nikolov, Darsh Wasan, Effects of micellar structuring and solubilized oil on the kinetic stability of aqueous foams, Ind. Eng. Chem. Res. 53 (49) (2014) 18891–18899, https://doi.org/10.1021/ie5014663.
[38] B. Petkova, S. Tcholakova, M. Chenkova, K. Golemanov, N. Denkov, D. Thorley, S. Stoyanov, Foamability of aqueous solutions: role of surfactant type and concentration, Adv. Colloid Interface Sci. 276 (2020), 102084, https://doi.org/10.1016/j.cis.2019.102084.
[39] M.J. Rosen, J. Solash, Factors affecting initial foam height in the Ross-Miles foam test, J. Am. Oil Chem. Soc. 46 (8) (1969) 399–402, https://doi.org/10.1007/BF02545623.
[40] S. Samanta, P. Ghosh, Coalescence of bubbles and stability of foams in aqueous solutions of Tween surfactants, Chem. Eng. Res. Des. 89 (11) (2011) 2344–2355, https://doi.org/10.1016/j.cherd.2011.04.006.

[41] H. Azira, A. Tazerouti, J.P. Canselier, Study of foaming properties and effect of the iomeric distribution of some anionic surfactants, J. Surfactants Deterg. 11 (4) (2008) 279–286, https://doi.org/10.1007/s11743-008-1093-3.
[42] O. Cheah, J.J. Cilliers, Foaming behaviour of Aerosol OT solutions at low concentrations using a continuous plunging jet method, Colloids Surf. A 263 (2005) 347–352, https://doi.org/10.1016/j.colsurfa.2005.01.011.
[43] N.D. Denkov, K.G. Marinova, S.S. Tcholakova, Mechanistic understanding of the modes of action of foam control agents, Adv. Colloid Interface Sci. 206 (2014) 57–67, https://doi.org/10.1016/j.cis.2013.08.004.
[44] P.R. Garrett, J.D. Hines, S.C. Joyce, P.T. Whittal, Report prepared for Unilever R&D, Port Sunlight, 1993.
[45] Rasband W.S., J. Image, U.S. National Institutes of Health Bethesda, Maryland, USA, ⟨http://rsb.info.nih.gov/ij⟩, 1997–2015.
[46] A. Scheludko, Thin liquid films, Adv. Colloid Interface Sci. 1 (1967) 391–464.
[47] Anabela Raymundo, José Empis, Isabel Sousa, Method to evaluate foaming performance, J. Food Eng. 36 (4) (1998) 445–452, https://doi.org/10.1016/S0260-8774(98)00063-6.
[48] W. Drenckhan, S. Hutzler, Structure and energy of liquid foams, Adv. Colloid Interface Sci. 224 (2015) 1–16, https://doi.org/10.1016/j.cis.2015.05.004.
[49] S.J. Neethling, H.T. Lee, P. Grassia, The growth, drainage and breakdown of foams, Colloids Surf. A 263 (2005) 184–196, https://doi.org/10.1016/j.colsurfa.2004.12.014.
[50] P. Grassia, S.J. Neethling, C. Cervantes, H.T. Lee, The growth, drainage and bursting of foams, Colloids Surf. A 274 (2006) 110–124, https://doi.org/10.1016/j.colsurfa.2005.08.040.
[51] Stefan Hutzler, D.örte Lösch, Enda Carey, Denis Weaire, Matthias Hloucha, Cosima Stubenrauch, Evaluation of a steady-state test of foam stability, Philos. Mag. 91 (4) (2011) 537–552, https://doi.org/10.1080/14786435.2010.526646.
[52] K.G. Marinova, N.D. Denkov, Foam destruction by solid-liquid antifoams in solutions of a nonionic surfactant: electrostatic interactions and dynamic effects, Langmuir 17 (2001) 2426–2436.
[53] S. Tcholakova, N.D. Denkov, T. Danner, Role of surfactant type and concentration for the mean drop size during emulsification in turbulent flow, Langmuir 20 (2004) 7444–7458, https://doi.org/10.1021/la049335a.
[54] S. Tcholakova, N.D. Denkov, D. Sidzhakova, I.B. Ivanov, B. Campbell, Interrelation between drop size and protein adsorption at various emulsification conditions, Langmuir 19 (2003) 5640–5649.